Functionalised Polyhedral Oligomeric Silsesquioxane with Encapsulated Fluoride – First Observation of Fluxional Si···F Interactions in POSS

Mathilde Laird,[a] Cedric Totée,[a] Philippe Gaveau,[a] Gilles Silly,[a] Arie Van der Lee,[b] Carole Carcel,[a] Masafumi Unno,[c] John R. Bartlett*[d] and Michel Wong Chi Man*[a]

[a]ICGM Univ. Montpellier, CNRS, ENSCM, Montpellier, France.
[b]Institut Européen des Membranes, Univ. Montpellier, CNRS, ENSCM, Montpellier, France
[c]Department of Chemistry and Chemical Biology, Graduate School of Science and Technology, Gunma University, Japan
[d]Western Sydney University, Locked Bag 1797, Penrith, NSW 2751, Australia.

Abstract : The synthesis of a styryl functionalised POSS incorporating an encapsulated fluoride ion within a $(SiO_{1.5})_8$ cage (T_8-F) is reported. It was characterised by single crystal XRD, MALDI-MS, FTIR, solution (^{29}Si, ^{19}F, ^{13}C, ^{1}H) and solid state (^{29}Si, ^{19}F) NMR. In the absence of ^{1}H decoupling, the ^{29}Si solution NMR spectrum exhibited a triplet of doublets. In contrast, ^{1}H, ^{19}F and ^{1}H/^{19}F double-decoupling resulted in two, three and one signal, respectively, being consistent with a single Si site whose ^{29}Si NMR signal is modulated by both the proximal aromatic-ring protons and fluoride. The associated Si···F coupling constant (2.3 Hz) is substantially lower than expected for a covalent Si-F bond and arises from a fluxional Si···F covalent effect in which the F^- interacts equivalently with all eight Si atoms. Additional variable temperature NMR studies demonstrated a threshold at -5 °C below which no Si···F interactions are observed, and above which an increasing Si···F covalent character occurs.

Introduction

The family of cage silsesquioxanes commonly referred to as polyhedral oligomeric silsesquioxanes (POSS) continue to attract significant interest within the materials chemistry community [1]. Hybrid T_n POSS compounds are composed of a well-defined polyhedral cage ($(SiO_{1.5})_n$, where n=8, 10, 12, etc, with n=8 being the most commonly reported) with the vertices covalently bonded to functional organic moieties [2, 3]. They can be readily transformed via different reactions on the organic group, including Heck coupling [4, 5], thiol-ene Click reaction [6], nitration [7], etc. The products obtained have been used in a wide variety of applications, including catalysis [8-11], optical and sensing applications [12-16], coating [17], etc. A particular feature of the POSS family is the presence of a central void within the cage, which was found to be around 0.3 nm in diameter by X-Ray single crystal diffraction in the case of T_8 cages [18-20]. This result was later confirmed in studies of a material incorporating T_8 POSS cages, where the size of the central void was measured at around 0.3 to 0.5 nm by positron annihilation lifetime spectroscopy and SAXS [21].

In 2003, Bassindale's group was the first to report the successful encapsulation of an ion (fluoride) within the central void of a T_8 silsesquioxane (T_8-F) [22]. In particular, after describing the synthesis of phenyl-functionalised T_8 via a reaction catalysed by tetrabutylammonium fluoride (TBAF) [18], they found that evaporation of the reaction solvent instead of precipitation of the product led to a new compound, which was unambiguously identified as octaphenyl-T_8 with a fluoride ion encapsulated within the cage. The octaphenyl T_8-F crystallised together with a tetrabutylammonium counter ion (located external to the cage) and was characterised by a silicon-fluorine distance of 2.65 Å. This distance is much longer than that generally observed for covalent Si-F bonds (1.71 Å) [22] or pentavalent Si-F species (1.67 Å) [23]. Complementary X-ray and NMR studies concluded that the fluorine was not covalently bonded, but was rather encapsulated as a "naked" anion with only minor perturbations in the structure of the T_8 host being observed [22]. Subsequent computational investigations demonstrated that the most favourable position for the fluoride in the T_8 structure is at the centre of the cage [24].

Later studies extended the range of available functionalised T_8-F compounds, and it has now been demonstrated that such systems can be readily synthesised with electron-withdrawing organic groups, but not with electron-donating species [25]. For example, in the case of organics with sp^2 hybridisation, the corresponding functionalised T_8-F compounds could be readily prepared [22, 26, 27]. In contrast, attempts to synthesise T_8-F cages functionalised with sp^3-hybridised organic groups (such as electron-donating alkyl substituents) yielded functionalised T_8 cages without encapsulated fluoride species. However, incorporating electron-withdrawing groups on the alkyl chains enabled the corresponding T_8-F compounds to be obtained, provided these groups were not good nucleofuges. Accordingly, T_8-F compounds functionalised with fluorinated alkyl chains have been described [28], in addition to analogues in which short alkyl moieties are terminated by strong electron-withdrawing groups such as cyano, acryloxy or acetoxy [25]. The role of the electron-withdrawing group in stabilising the T_8-F structure was attributed to the fact that in π-delocalised systems, the LUMO and HOMO are located outside of the cage. The centre of the cage would thus be positively charged, stabilising the fluoride anion [25, 26]. In contrast, in the case of electron-donating groups, the

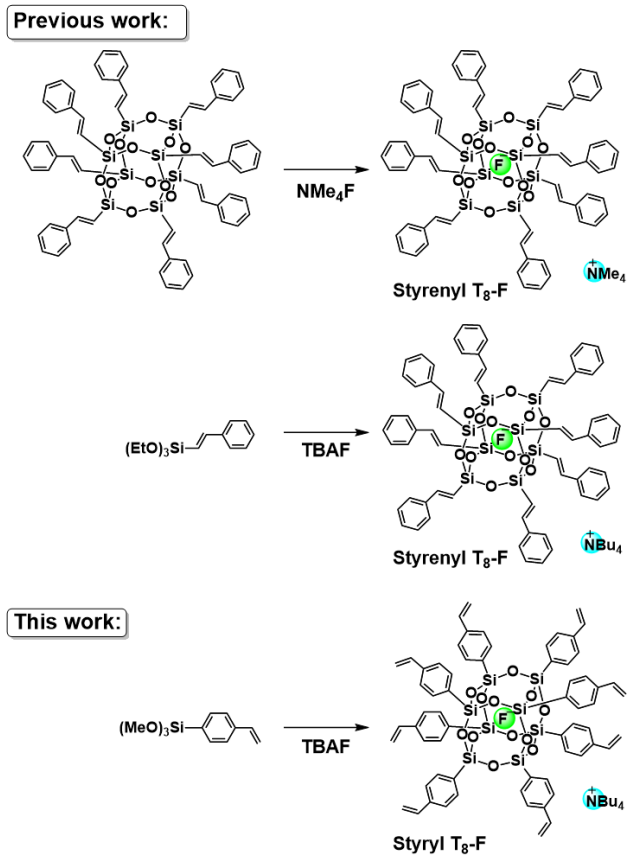


Fig. 1 Synthetic routes to styrenyl- and styryl-functionalised T_8-F silsesquioxanes.

LUMO and HOMO are located within the cage, resulting in a negatively-charged cage which would destabilise the fluoride anion [29].

We recently reported the synthesis and characterisation of a new family of styryl-functionalised T_n POSS compounds (n=8, 10, 12 or 18), in which the styryl group was linked to the cage via the phenylene group rather than the vinyl group [30-32]. Such POSS compounds with organic moieties can be further modified via reactions such as hydrosilylation, Heck coupling, thiol-ene Click reactions, metathesis, etc, without modifying the structure of the T_n core. They are of particular interest, since they expand the range of potential applications described above. As previously reported by Bassindale et al. [22], we have also found that changes in the work-up technique lead to a different product, which has been unambiguously identified as a styryl-functionalised T_8-F compound. Similarly to our previously reported styryl-functionalised T_n compounds, T_8-F cages with styrenyl moieties anchored via the vinylic group have previously been reported (Fig. 1) [26, 28]. However, in all earlier reports, the vinylphenyl moiety linked to the silsesquioxane cage via the vinylic C=C bond precludes further functionalisation of the latter.

Here, we present the synthesis of a new styryl-functionalised T_8-F, in which the organic function is linked to the cage by the phenylene group. The structure of the new precursor is described, based on X-ray crystallography, multinuclear liquid and solid-state NMR, mass spectrometry and infrared spectroscopy. An unusual and previously undocumented fluxional interaction between the silicon atoms of the T_8 cage and the encapsulated fluoride ion is also demonstrated, based on the results of double-decoupling (^{1}H and ^{19}F) ^{29}Si NMR studies.

Results and Discussion

Synthesis of styryl-functionalised T_8-F

The synthetic protocol used to prepare styryl-functionalised T_n compounds (n=8, 10, 12 and 18) has been previously described in detail [30, 31]. In the present study, and as previously found by Bassindale et al. [22], we found that changes in the work-up technique lead to a significantly different mixture of products, which are also obtained in higher yields than the fluoride-free T_n compounds obtained in our earlier studies. In particular, in the current study, TBAF is not sequestered by $CaCl_2$, and part of it remains associated with the cage. The excess was removed by washing with water.

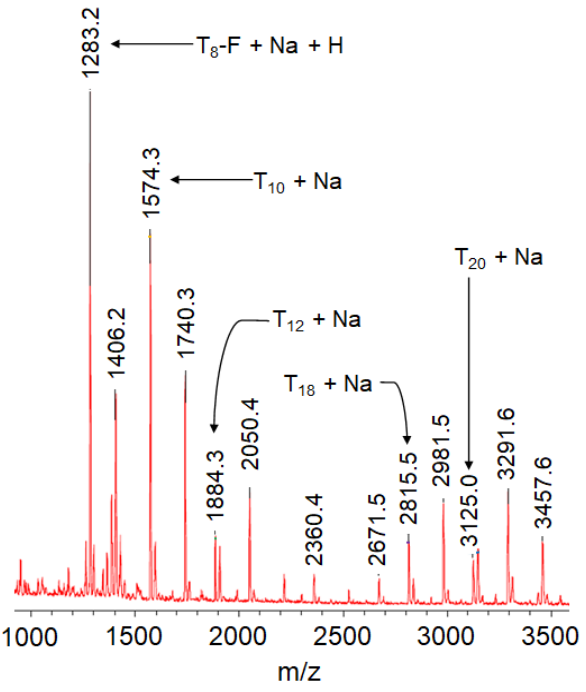


Fig. 2 MALDI mass spectrum of the crude reaction product obtained from the modified cage silsesquioxane synthesis.

The MALDI mass spectrum of the resulting product mixture is illustrated in Fig. 2. The spectrum exhibits mass peaks corresponding to the expected styryl-functionalised T_{10} and T_{12} cages (T_n+Na), together with those of larger cages such as the corresponding T_{18}, T_{20} (with the expected incremental value of 310 m/z between T_n and T_{n+2}, where 310 m/z corresponds to the mass of $(C_8H_7SiO_{1.5})_2$), and partially-condensed products. However, no peak corresponding to the expected T_8 product (for which m/z=1263.2 for T_8+Na [30]) was evident. Instead, depending on the desorption matrix used (see ESI), a well-defined peak is observed at either m/z=1283.2 (attributed to T_8-F + Na + H, with dithranol and sodium trifluoroacetate as desorption matrix) or m/z=1282.2 (attributed to T_8-F + Na, with dithranol alone), which is 19-20 m/z higher than the expected mass. These data are consistent with the formation of a T_8 cage associated with a fluoride anion. Since the styryl group is strongly electron withdrawing, it was probable that the new product was a styryl-functionalised T_8-F cage [22]. After re-dissolving the crude production in toluene, a precipitate was spontaneously formed, which was separated from the solvent and washed with cold toluene. The white powder, which was obtained with 26 % yield, was recrystallised from a dichloromethane/toluene solvent mixture to yield crystals suitable for single-crystal X-ray diffraction studies. The MALDI mass spectrum of the recrystallised product, Fig. S1, confirmed that a single product, with m/z=1283.2, was obtained. This mass is consistent with T_8-F + Na + H rather than T_8-F + TBA, indicating that an ion-exchange reaction occurred during the MALDI measurement.

Structure of styryl-functionalised T_8-F

The single-crystal X-ray diffraction structure of the pure product is illustrated in Fig. 3, while the lattice parameters are summarised in Table S1. The structure is characterised by two non-equivalent T_8 cages, each with an encapsulated fluoride anion, which co-crystallise with TBA^+ counter ions and solvent molecules. Due to the mobility of the solvent molecules, the latter do not appear clearly in the structure. In one cage, the fluoride ion is located on the centre-of-symmetry of the T_8 cage (left-hand cage in Fig. 3), whereas in the other non-equivalent cage, the fluoride is located slightly off-centre (right-hand cage in Fig. 3). This is somewhat different to the structure reported by Bassindale et al. for phenyl-functionalised T_8-F, in which all T_8-F cages were structurally equivalent [22]. The distances between the silicon and fluoride in each cage are shown in Fig. S2. The average Si···F distance is essentially identical for both cages (2.65 Å) and is in excellent agreement with the Si···F distance in the phenyl-functionalised system (2.65 Å [22]) and a variety of other organo-functionalised T_8-F compounds (2.64-

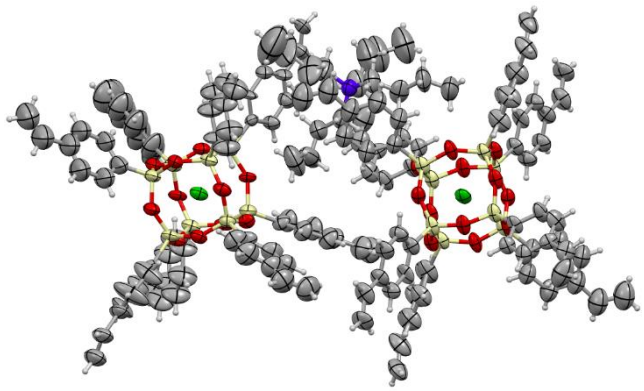


Fig. 3 X-ray crystal structure of styryl-functionalised T_8-F cage silsesquioxane. Yellow = Si, red = O, purple = N, green = F, grey = C, white = H.

2.66 Å) [25]. However, the range of values is much higher in the case of the off-centre fluoride (2.58-2.72 Å, compared to 2.64-2.68 Å for the cage where the fluoride is located on the centre-of-symmetry). Here again, it is noteworthy that the Si···F distance differs significantly from those observed in regular Si-F covalent bonds (1.71 Å) [22]. The other characteristic bond distances and bond angles are compared with those of the corresponding styryl-functionalised T_8 silsesquioxane in Table 1. As previously found for the phenyl-functionalised T_8-F silsesquioxane [22], only minor perturbations are evident in the structure of the T_8 cage, with the silicon atoms pulled more closely together, and the oxygen atoms pushed slightly apart due to the presence of the fluoride in the T_8-F cage.

The FTIR spectrum (Fig. S3) of styryl-functionalised T_8-F powder exhibits the characteristic bands related to the styryl moieties, including ν(C=C) and $\nu(C{=}C)_{ring}$ stretching at 1628 and 1600 cm^{-1}, respectively. In addition, the narrow band at 1079 cm^{-1} corresponding to the Si-O-Si stretching mode confirms the presence of a well-defined cage silsesquioxane rather than a polymer. The sharpness of this peak, compared to that of the corresponding T_8 material, is striking and suggests that the T_8 cage in styryl-functionalised T_8-F is in a more symmetrical environment than in the corresponding styryl T_8.

Multinuclear NMR characterisation of styryl-functionalised T_8-F

Multinuclear NMR techniques provide rich insights into the structure and dynamics of functionalised POSS systems, particularly for investigating the effect of the encapsulated fluoride anion on the cage structure and the speciation of the fluoride ion itself. The ^1H NMR spectrum of the styryl-functionalised T_8-F is significantly different to that of the corresponding T_8 system, especially with respect to the chemical shifts of the aromatic protons (Fig. 4). In particular, the latter are shifted from 7.72-7.70 and 7.41-7.38 ppm for the T_8 system to 7.75-7.73 and 7.32-7.30 ppm, respectively, for T_8-F. The vinylic signals are impacted by the presence of fluoride to a lesser extent. In addition, the spectrum of T_8-F exhibits signals arising from the TBA^+ ion at 1.92, 1.01, 0.80 and 0.73 ppm (Fig. S4). As expected, the integration across the full spectrum is consistent with the presence of one TBA^+ ion per T_8-F cage.

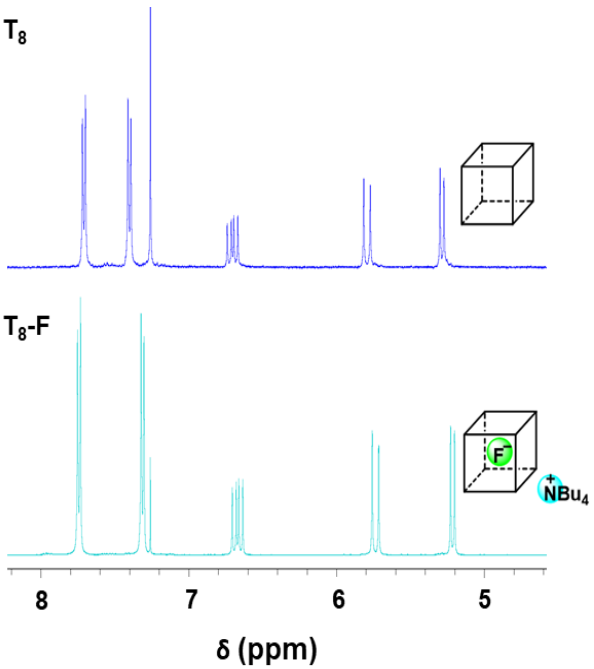


Fig. 4 Solution ^1H NMR spectra in $CDCl_3$ of styryl-functionalised T_8-F (bottom) (excluding signals arising from TBA^+ below 2 ppm) and T_8 (top).

Table 1 Characteristic bond distances and bond angles in styryl-functionalised T_8-F and T_8.

	Styryl T_8			Styryl T_8-F		
	min	**average**	**max**	**min**	**average**	**max**
Si-O bond (Å)	1.603	1.617	1.631	1.591	1.620	1.638
Si-C bond (Å)	1.827	1.841	1.852	1.760	1.829	1.860
Si···Si distance[a] (Å)	5.361	5.388	5.415	5.277	5.300	5.367
Si···F distance (Å)	*n.a*	*n.a*	*n.a*	2.575	2.651	2.717
Si-O-Si angle (°)	138.6	149.1	161.5	139.7	141.6	144.1
O-Si-O angle (°)	107.5	109.1	110.2	110.5	112.6	115.2

[a] diagonal distance between opposite corner
n.a, not applicable

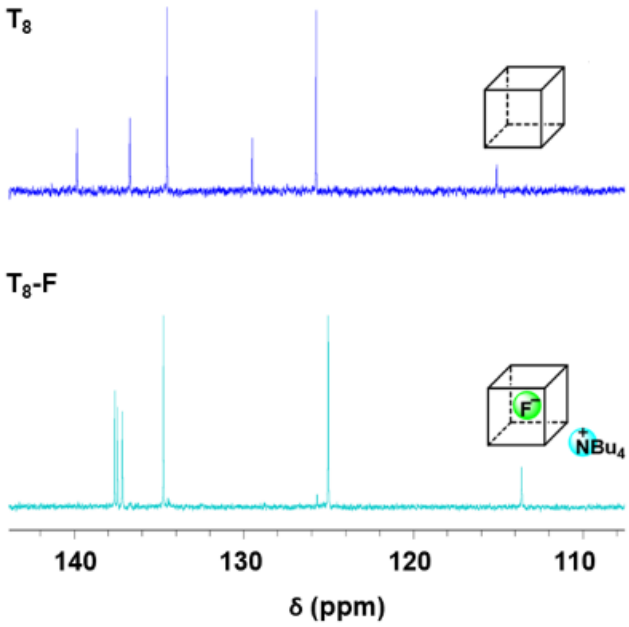


Fig. 5 Solution ^{13}C-{^1H} NMR spectra of styryl-functionalised T_8-F (bottom) and T_8 (top) in $CDCl_3$.

The ^{13}C-{^1H} solution NMR spectrum of the styryl groups is strongly affected by the presence of the fluoride within the cage (Fig. 5), particularly the signal arising from the quaternary aromatic carbon directly linked to the silicon atoms. For example, the latter shifts from 129.56 ppm in styryl-functionalised T_8 to around 137 ppm for the corresponding T_8-F system. The second quaternary carbon, linked to the vinyl moiety, is also impacted and the corresponding signal shifts from 139.92 to around 137 ppm. In the T_8-F system, the explicit attribution of signals to the two quaternary carbons is complicated due to their similar chemical shifts, which are observed at 137.41 and 137.58 ppm. The vinylic carbon linked to the aromatic ring was identified by its signal at 137.13 ppm in the spectrum of T_8-F using a Distortionless Enhancement by Polarisation Transfer (DEPT) 135 NMR sequence. The vinylic and tertiary aromatic carbon atoms are less impacted by the presence of fluoride. Signals arising from the TBA^+ counterion are observed at 58.30, 23.43, 19.50 and 13.75 ppm.

The ^{19}F-{^1H} solution NMR signal observed at -25.17 ppm (Fig. 6) is characteristic of fluoride encapsulated in T_8 cages (typically observed at -24 to -30 ppm) [2, 22, 25]. It should be noted that TBAF typically gives rise to a signal at -73 to -146 ppm [22]; no such resonance is evident in our case (Fig. 6), confirming that the fluoride is encapsulated within the silsesquioxane cage.

Fig. 7 presents the ^{29}Si-{^1H} solution NMR spectrum of styryl-functionalised T_8-F. Two signals are observed at -81.48 and -81.52 ppm, which appear upfield by 3.3 ppm compared with the signal for the corresponding T_8 system (-78.19 ppm [30]). Such differences are typically observed between T_8 and T_8-F silsesquioxanes bearing the same organic substituents [25]. However, to our knowledge, this is the first time that two ^{29}Si signals have been observed in such a T_8-F system, and in particular the corresponding

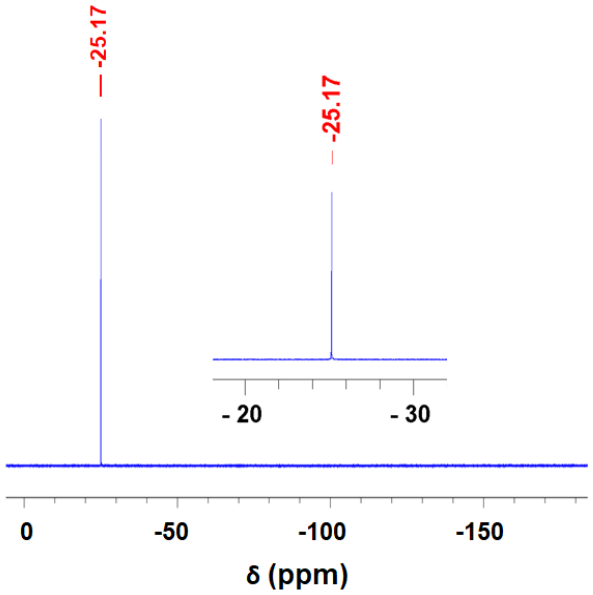


Fig. 6 Solution ^{19}F-{^{1}H} NMR spectra of styryl-functionalised T_8-F in $CDCl_3$. Inset: expanded view of the region from -20 to -30 ppm, illustrating the singlet arising from the encapsulated fluoride.

phenyl-functionalised system only exhibits a single signal at -80.6 ppm [22]. The upfield shift in the case of the phenyl-functionalised system is also smaller (0.9 ppm [22]), due presumably to the stronger electron withdrawing effect of the styryl substituent.

Given the observation of two signals in the proton-decoupled ^{29}Si solution NMR spectrum, it is of interest to probe the origins of this effect. As indicated above, two non-equivalent T_8-F cages are observed in the solid state via single crystal X-ray diffraction studies, and hence it is tempting to attribute the two discrete ^{29}Si NMR signals in the solution spectrum to these non-equivalent environments. However, X-ray diffraction crystallography measures the location of the atoms in the solid state where movements are limited, whereas the solution NMR experiment is probing a system with significantly greater translational and rotational "freedom". In addition, under the hypothesis that the two non-equivalent environments could be distinguished in liquid NMR, at least two ^{29}Si signals would arise from the fluoride-off-centred cage and one from the cage with the fluoride located on the centre of symmetry. These effects would be seen in both the ^{29}Si and ^{19}F solution NMR spectra (with multiple signals potentially being observed in ^{29}Si and ^{19}F NMR, unless the respective signals are too close to be resolved under the conditions used here). However, only two signals are observed in ^{29}Si NMR, together with a single signal in ^{19}F NMR. Following these observations, further decoupling experiments were undertaken in order to investigate the role of the fluoride in such interactions and to determine if the two signals observed in the liquid ^{29}Si NMR spectrum are due to two silicon-atom environments in the cage or to Si-F coupling.

The coupling constant typically observed for covalent Si-F species ranges from 250 to 300 Hz [33]. Here, we observe two signals separated by only 2.5 Hz in the case of the ^{29}Si

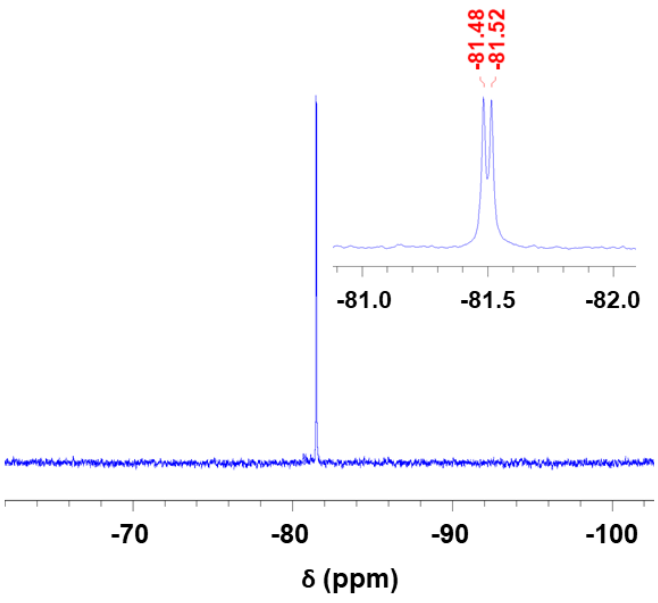


Fig. 7 Solution ^{29}Si-{^{1}H} NMR spectra of styryl-functionalised T_8-F in $CDCl_3$. Inset: expanded view of the region from -81 to -82 ppm.

solution NMR proton-decoupled spectrum, indicating that the interaction between Si and F differs significantly from a conventional covalent bond. It was also observed that the separation between the signals varies depending on the NMR solvent; a separation of 2.5 Hz was observed in $CDCl_3$ while the separation was only 0.85 Hz in DMF-d_7 at ambient temperature. To further probe the role of coupling in the styryl-functionalised T_8 system, four different ^{29}Si NMR sequences were investigated:

- ^{29}Si NMR without any decoupling;
- ^{29}Si NMR with ^{1}H decoupling;
- ^{29}Si NMR with ^{19}F decoupling;
- ^{29}Si NMR with double decoupling (both ^{1}H and ^{19}F).

In the absence of decoupling, the ^{29}Si NMR spectrum exhibits a complex signal profile consisting of a triplet of doublets (Fig. 8). Two coupling constants can be extracted from this spectrum, with values of 5.89 and 2.06 Hz. After ^{1}H decoupling (^{29}Si-{^{1}H} in Fig. 8), a doublet is observed with a coupling constant of 2.5 Hz (which is close to 2.06 Hz and is hence attributed to the same interaction). The 5.89 Hz coupling constant is thus attributed to ^{1}H coupling which can reasonably be assigned to Si coupling with the CH_β protons of the aromatic ring. When ^{19}F decoupling is performed (^{29}Si-{^{19}F} in Fig. 8), the spectrum now exhibits a triplet with a coupling constant of 5.89 Hz, suggesting that the 2.5 Hz coupling constant arises from Si coupling with F. Finally, when a double decoupling of ^{1}H and ^{19}F was undertaken (^{29}Si-{^{1}H,^{19}F} in Fig. 8), only a singlet was observed, demonstrating that the ^{29}Si NMR signals from the silicon atoms in the cage are influenced by both the proximal protons on the aromatic rings and the encapsulated fluoride anion. In addition, the success of the decoupling experiments precludes the possibility that the two signals could arise from spatial interactions, since fluoride decoupling only affects scalar interactions. The presence of a single signal in the ^{29}Si liquid NMR spectrum after the double decoupling experiment indicates that only one silicon environment is observed in the ^{29}Si solution NMR experiment.

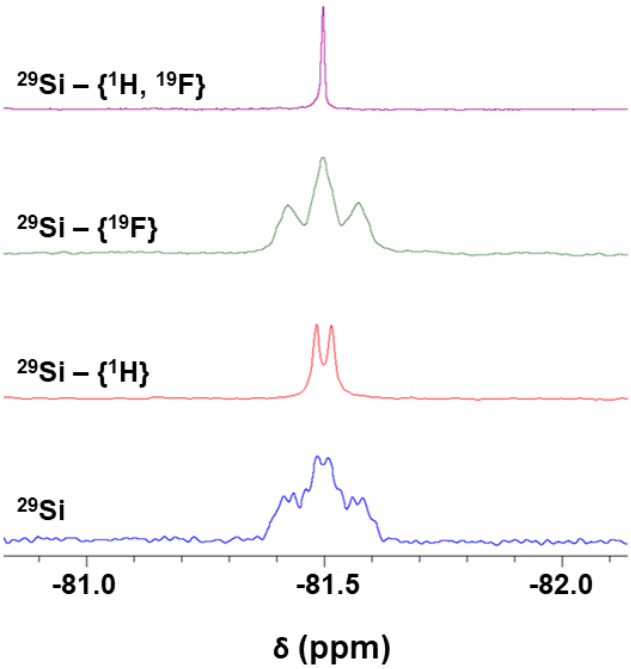


Fig. 8 Solution ^{29}Si NMR spectra in $CDCl_3$ of styryl-functionalised T_8-F using different decoupling sequences.

For completeness, we have also recorded the ^{29}Si NMR spectra using various NMR probes and at different magnetic field strengths (9.4 T (400 MHz) and 11.8 T (500 MHz)), to confirm these attributions. The results obtained are presented in Fig. S5 (note that the horizontal axis is calibrated in Hz rather than ppm, to facilitate a

meaningful comparison of the J coupling values obtained under different conditions). These data demonstrate that with ^{1}H decoupling only (^{29}Si-{^{1}H}), the magnitude of the splitting is always the same within experimental error, with the doublet centred on the position of the single ^{29}Si-{^{1}H,^{19}F} signal. This is consistent with the above attribution of the observed ^{29}Si NMR signals.

As a single fluoride anion is present in each cage and a single signal (i.e. a single population of silicon atoms) is observed in ^{29}Si solution NMR after decoupling, it is evident that the fluoride ion interacts equivalently with all eight silicon atoms of the cage. As indicated above, the $J_{Si\text{-}F}$ coupling constant observed here (2.5 Hz) is significantly lower than that commonly observed for typical Si-F covalent interactions (250-300 Hz) [33], indicating that the interaction is not a conventional covalent bonding. Fluxional silicon-fluoride interactions were described by Brondani et al. in heptafluorinated trisilacyclohexane [34], in which each silicon atom was functionalised with two fluorine atoms and was impacted by the effects of an additional intra-cyclic fluoride anion. An average of these interactions was measured by NMR, leading to a reported coupling constant of 85.5 Hz. Here, we also conclude that the Si···F interaction in the case of styryl-functionalised T_8-F is a fluxional covalent bonding (Fig. 9) and that on the time scale of the NMR measurement an average value of these interactions is observed, resulting in a low coupling constant. The coupling constant observed for styryl-functionalised T_8-F is much smaller than that observed by Brondani et al., due to the different interaction forces and geometry. In particular, the fluoride anion is exchanging on only three silicon atoms in the latter system compared to eight silicon sites in the styryl-functionalised T_8-F. It is of interest to note that no measurable Si-F coupling was reported in the case of the corresponding phenyl-functionalised system [22], indicating that the Si···F interactions are stronger in the case of the styryl-functionalised system due presumably to the stronger electron-withdrawing effect of the styryl group. Interestingly, the fluxional covalent Si···F interaction is consistent with the single crystal X-ray observation of the Si···F distance (see above), which is nearly 1 Å longer than a regular covalent Si-F bond.

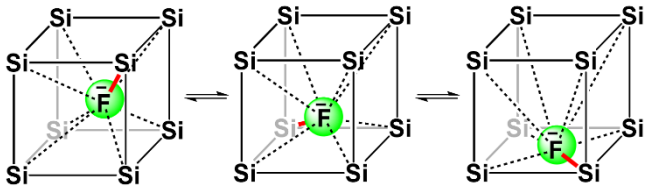


Fig. 9 Possible fluxional covalent bonding representation for T_8-F. Black and grey lines = Si-O-Si bond; red line = covalent bond at a particular time, t; black dashed line = future covalent bond at time t+δt, where δt is small compared to the time scale of the NMR experiment

Due to the presence of a $J_{Si\text{-}F}$ coupling constant in the ^{29}Si NMR spectrum, a corresponding $J_{F\text{-}Si}$ coupling constant might be expected in the ^{19}F NMR spectrum. However, given the very low coupling constant value ($J_{Si\text{-}F}$ = 2.5 Hz), the low relative abundance of ^{29}Si compared to ^{19}F (4.68 and 100.00 % respectively) and the width of the ^{19}F signal (full width at half maximum = 1.92 Hz), the signal appears only as a singlet in the ^{19}F NMR spectrum.

Solid state NMR studies provide additional insights into the differences between the structures of the functionalised T_8-F system in the solid state and in solution and enable the environment of the encapsulated fluoride anion to be further probed. The ^{19}F solid

state NMR spectrum exhibits a single signal at -24.9 ppm (Fig. 10, top), which is close to that observed in solution (-25.17 ppm, Fig. 6). This suggests that the fluoride ions are effectively "shielded" from their external environment, as also previously reported for the corresponding phenyl-functionalised system [22]. In contrast, the ^{29}Si NMR spectrum (Fig. 10, bottom) reveals the presence of two signals at -80.7 and -81.2 ppm separated by 30.7 Hz. This doublet could either arise from a fluxional Si···F interaction (as observed in liquid NMR studies above) or from the presence of two non-equivalent silicon sites in the solid state (as also observed by X-ray crystallography). Double-decoupling experiments indicated that two signals are retained even when decoupling pulse sequences are employed. Hence, the two signals observed in the solid state are tentatively attributed to the presence of two non-equivalent silicon environments.

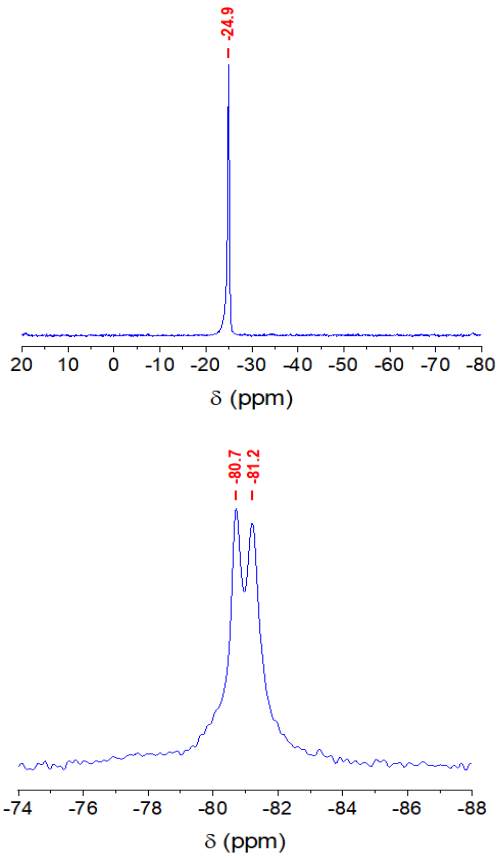


Fig. 10 ^{29}F SP-MAS (top) and ^{29}Si CP-MAS (bottom) solid state NMR spectra of styryl-functionalised T_8-F.

^{29}Si variable temperature NMR study

To further probe the dynamics of the styryl-functionalised T_8-F system, a variable-temperature ^{29}Si liquid NMR study was undertaken using DMF-d_7 as solvent, at temperatures from -55 to 115 °C as illustrated in Fig. 11. Given the doublet described above in the ^{29}Si NMR spectrum, a coalescence of the two signals might be anticipated at sufficiently high temperatures, due to an increased rate of exchange between the various conformers in the system [35, 36]. In addition, it might be expected that decreasing temperature would lead to the entrapped fluoride interacting with a single silicon atom at sufficiently low temperature, leading to the emergence of two sets of ^{29}Si signals; one arising from the silicon species no longer interacting with fluoride, and a second arising from the silicon interacting with fluoride (exhibiting an increased $J_{Si\text{-}F}$). Instead, a singlet is observed in the ^{29}Si spectrum from -55 to -15 °C (Fig. 11), with a doublet clearly observed above

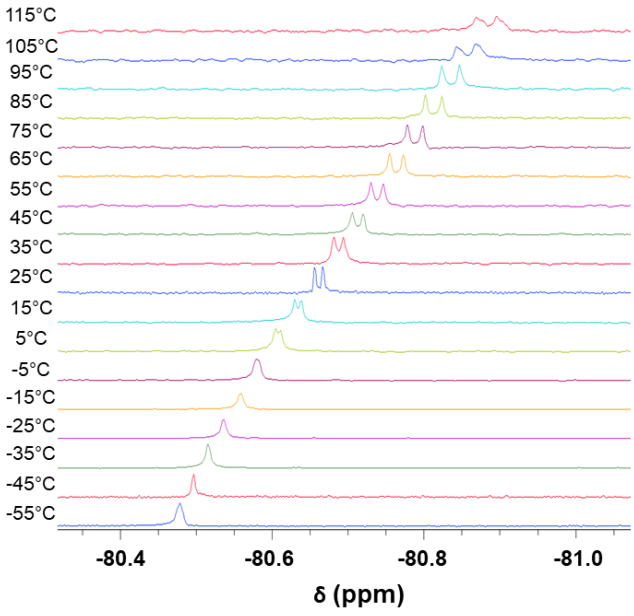


Fig. 11 Variable temperature solution ^{29}Si-{^{1}H} NMR spectra of styryl-functionalised T_8-F in DMF-d_7.

5 °C which exhibits a J_{Si-F} coupling constant increasing linearly from 0.47 to 2.21 Hz between 5°C and 115 °C in DMF-d_7. Additional ^{1}H decoupled and ^{1}H-^{19}F double-decoupled experiments carried out at -55 °C did not enable any signals arising from a possible Si-F covalent interaction (which might result from fixing of the fluoride anion on one silicon corner at low temperature), to be identified. The observation of a singlet at low temperature can thus be attributed to the absence of interactions of the fluoride with the silicons at low temperature, resulting in a "frozen" system where the fluoride is isolated in the centre of the cage with too large a Si···F distance to allow substantial orbital overlapping and J coupling interactions. Between -5 and 5°C, a transition occurs, where the "frozen" fluoride clearly engages in the expected fluxional covalent interaction with the eight silicon atoms, for which we observe a coupling constant J_{Si-F} = 0.47 Hz at 5 °C in DMF-d_7. With increasing temperature, F atoms spend more time in the vicinity of Si atoms and the covalent character of the interaction becomes stronger, leading to a corresponding increase in J_{Si-F} with increasing temperature (J_{Si-F} = 2.21 Hz at 115 °C).

To investigate the possibility of ion-pairing interaction between the encapsulated fluoride anion and the TBA counterion, which might be expected to vary with temperature, the ^{1}H NMR spectrum of the system was also obtained as a function of temperature (see Fig. S6). Neither the positions of the signals between 0 and 3.5 ppm (arising from the TBA counterion), nor the corresponding J couplings extracted from the multiplets, show any anomalous behaviour with temperature. In addition, we note that the variations in line shape in Fig. S6 with temperature are a consequence of the fact that the spectrometer magnet was shimmed at ambient temperature. As is well known, ^{1}H NMR signals are very sensitive to shim quality which degrades with variations in temperature. On the basis of these data we conclude that there is no evidence for specific ion-pairing interactions between the encapsulated fluoride and the (external) TBA counterion.

Extraction of fluoride from the T_8 cage

As indicated above, changes in the workup procedure initially used to produce styryl-functionalised T_8 silsesquioxanes lead to the formation of the corresponding T_8-F compound, which is obtained in significantly higher yields than the former product (26 and 5.7 %, respectively). This observation suggests that removal of the fluoride from the T_8-F system might lead to improved yields of the T_8 product if quantitative removal of the fluoride anion from T_8-F is feasible.

Several possible approaches for removing the fluoride ion from functionalised T_8-F cages have been previously investigated [25, 28, 37]. Following the approaches reported in these earlier studies, the styryl-functionalised T_8-F was dissolved in THF and then stirred in the presence of either LiCl or $CaCl_2$ or washed with a saturated solution of $CaCl_2$. None of these approaches led to the removal of the fluoride ion, even after six days of reaction or microwave irradiation. In addition, treating the T_8-F with trifluoroacetic acid was also investigated, as previously described for other T_8-F systems [25], but cage cleavage was observed in our system. Hence, we conclude that in the case of the

styryl-functionalised T_8 cage silsesquioxane, the fluoride cannot be readily extracted without breaking the T_8 cage, further confirming the high stability of the styryl-functionalised T_8-F system. The observation that the fluoride cannot be removed in our system using the previously described conditions is consistent with stronger Si···F interactions in the case of the styryl T_8-F. This is also evident from the significant ^{29}Si chemical shift between T_8 and T_8-F and the observation of a Si···F fluxional interaction, which has not been previously described for organo-functionalised T_8-F systems.

Following earlier work [38], we observed that if $CaCl_2$ was added to the reaction mixture prior to the evaporation step during workup, then no T_8-F is obtained (due presumably to sequestering of the fluoride anion by Ca^{2+}). In contrast, once the solvent is evaporated, the fluoride is irreversibly trapped within the cage to form T_8-F, and post-treatment with $CaCl_2$ can no longer sequester the trapped anion. This effect was studied by ^{1}H solution NMR, and the spectra of the crude reaction product before and after $CaCl_2$ treatment are presented in Fig. 12. Before addition of $CaCl_2$, a mixture of silsesquioxanes is evident (Fig. 12, bottom) which cannot be readily distinguished. However, after treatment with $CaCl_2$ (and sequestering of fluoride), T_8, T_{10} and T_{12} silsesquioxanes were identified by ^{1}H NMR (Fig. 12, top). In particular, no signals attributable to T_8-F were evident under these conditions, confirming the role of fluoride sequestration in suppressing the formation of T_8-F.

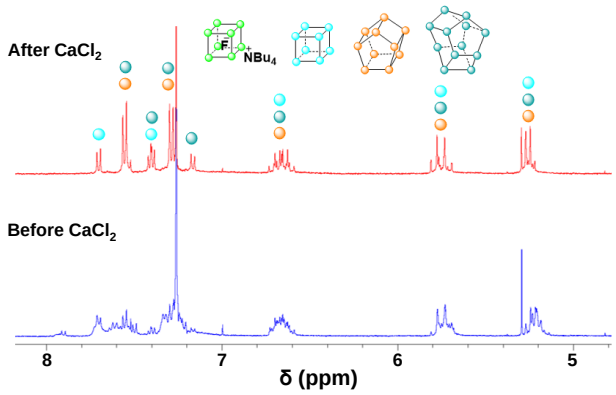


Fig.12 ^{1}H solution NMR spectra of the crude reaction product before (bottom) and after $CaCl_2$ treatment (top) in $CDCl_3$.

Conclusions

In summary, we report the synthesis and characterisation of a new styryl-functionalised T_8 cage silsesquioxane containing an encapsulated fluoride anion, thus extending the range of functional organic moieties available in the T_8-F POSS family. The structure of the styryl-functionalised T_8-F was solved by single crystal X-ray diffraction, which highlighted the presence of two distinct cages in the solid state; one in which the fluoride anion is located on the centre-of-symmetry and a second in which the fluoride is located off-centre. A multinuclear liquid NMR study (^{29}Si, ^{19}F and ^{1}H) revealed the presence of a coupling constant, $J_{Si\text{-}F}$ between the silicon atoms and the encapsulated fluoride in T_8-F solutions. The unprecedented low value of the latter at ambient temperature ($J_{Si\text{-}F}$ = 2.5 Hz in $CDCl_3$; 0.85 Hz in DMF-d_7) compared to values more commonly observed for covalent Si-F bonding (250 to 300 Hz) is indicative of a dynamic interaction between the silicon and fluorine atoms. This was attributed to fluxional covalent bonding between the fluoride and the eight silicon atoms. The latter was investigated by variable temperature ^{29}Si NMR studies, which demonstrated the absence of Si···F interactions below a temperature threshold of -5 °C and an increasing

covalent character of the Si···F fluxional interaction beyond that threshold temperature. To the best of our knowledge, this is the first report of such intriguing phenomena in functionalised T_8-F compounds.

Moreover, previously reported approaches for removing the fluoride from organo-functionalised T_8-F cages, without cage cleavage, were also investigated. Under the range of conditions tested, it was found that the fluoride anion could not be extracted from styryl-functionalised T_8-F without cleavage, in contrast to earlier reports of the successful removal of fluoride from other functionalised T_8-F compounds. This highlights the strength of the Si···F interactions in the styryl-functionalised T_8-F compound (which are also observed via NMR) and its relatively high stability compared to other common organo-functionalised T_8-F compounds.

We are currently investigating approaches for converting the styryl-functionalised T_8-F precursor into hybrid materials via sol-gel processing; this work will be reported in a future paper.

Acknowledgements

The authors gratefully acknowledge Emmanuel Fernandez (Laboratoire de Mesures Physiques, Université de Montpellier, Ecole Nationale Supérieure de Chimie de Montpellier) for solid-state NMR experiments. Funding from the French Ministère de l'Enseignement Supérieur et de la Recherche to support the PhD scholarship of ML and the Japan Student Services Organization for a travel scholarship awarded to ML are gratefully acknowledged.

Notes and references

1. Y. Du and H. Liu, *Dalton Trans.*, 2020, **49**, 5396-5405.
2. D. B. Cordes, P. D. Lickiss and F. Rataboul, *Chem. Rev.*, 2010, **110**, 2081-2173.
3. R. M. Laine, *J. Mater. Chem.*, 2005, **15**, 3725-3744.
4. S. Sulaiman, A. Bhaskar, J. Zhang, R. Guda, T. Goodson III and R. M. Laine, *Chem. Mater.*, 2008, **20**, 5563-5573.
5. M. Y. Lo, K. Ueno, H. Tanabe and A. Sellinger, *Chem. Rec.*, 2006, **6**, 157-168.
6. L. A. Bivona, O. Fichera, L. Fusaro, F. Giacalone, M. Buaki-Sogo, M. Gruttadauria and C. Aprile, *Catal. Sci. Technolog.*, 2015, **5**, 5000-5007.
7. Y. Ni, S. Zheng and K. Nie, *Polymer*, 2004, **45**, 5557-5568.
8. E. A. Quadrelli and J. M. Basset, *Coord. Chem. Rev.*, 2010, **254**, 707-728.
9. F. Giacalone and M. Gruttadauria, *ChemCatChem*, 2016, **8**, 664-684.
10. L. A. Bivona, F. Giacalone, E. Carbonell, M. Gruttadauria and C. Aprile, *ChemCatChem*, 2016, **8**, 1685-1691.
11. Y. Zhou, G. Yang, C. Lu, J. Nie, Z. Chen and J. Ren, *Catal. Commun.*, 2016, **75**, 23-27.
12. S. Chanmungkalakul, V. Ervithayasuporn, P. Boonkitti, A. Phuekphong, N. Prigyai, S. Kladsomboon and S. Kiatkamjornwong, *Chem. Sci.*, 2018, **9**, 7753-7765.
13. S. Chanmungkalakul, V. Ervithayasuporn, S. Hanprasit, M. Masik, N. Prigyai and S. Kiatkamjornwong, *Chem. Commun.*, 2017, **53**, 12108-12111.
14. H. Zhou, Q. Ye and J. Xu, *Mater. Chem. Front.*, 2017, **1**, 212-230.
15. A. Sellinger, R. Tamaki, R. M. Laine, K. Ueno, H. Tanabe, E. Williams and G. E. Jabbour, *Chem. Commun.*, 2005, DOI: 10.1039/b505048k, 3700-3702.
16. L. Sun, Y. Liu, S. Dang, Z. Wang, J. Liu, J. Fu and L. Shi, *New J. Chem.*, 2016, **40**, 209-216.

17. F. Ciesielczyk, K. Szwarc-Rzepka, M. Przybysz, J. Czech-Polak, M. Heneczkowski, M. Oleksy and T. Jesionowski, *Colloids Surf. A Physicochem. Eng. Asp.*, 2018, **537**, 557-565.
18. A. R. Bassindale, Z. Liu, I. A. MacKinnon, P. G. Taylor, Y. Yang, M. E. Light, P. N. Horton and M. B. Hursthouse, *Dalton Trans.*, 2003, DOI: 10.1039/b302950f, 2945-2949.
19. N. Hurkes, C. Bruhn, F. Belaj and R. Pietschnig, *Organometallics*, 2014, **33**, 7299-7306.
20. M. A. Hossain, M. B. Hursthouse and K. M. A. Malik, *Acta Crystallogr., Sect. B*, 1979, **B35**, 2258-2260.
21. C. Zhang, F. Babonneau, C. Bonhomme, R. M. Laine, C. L. Soles, H. A. Hristov and A. F. Yee, *J. Am. Chem. Soc.*, 1998, **120**, 8380-8391.
22. A. R. Bassindale, M. Pourny, P. G. Taylor, M. B. Hursthouse and M. E. Light, *Angew. Chem. Int. Ed.*, 2003, **42**, 3487-3490.
23. F. H. Carré, R. J. P. Corriu, C. Guérin, B. J. L. Henner and W. W. C. Wong Chi Man, *J. Organomet. Chem.*, 1988, **347**, C1-C4.
24. J. A. Tossell, *J. Phys. Chem. C*, 2007, **111**, 3584-3590.
25. Y. El Aziz, A. R. Bassindale, P. G. Taylor, P. N. Horton, R. A. Stephenson and M. B. Hursthouse, *Organometallics*, 2012, **31**, 6032-6040.
26. S. E. Anderson, D. J. Bodzin, T. S. Haddad, J. A. Boatz, J. M. Mabry, C. Mitchell and M. T. Bowers, *Chem. Mater.*, 2008, **20**, 4299-4309.
27. A. R. Bassindale, D. J. Parker, M. Pourny, P. G. Taylor, P. N. Horton and M. B. Hursthouse, *Organometallics*, 2004, **23**, 4400-4405.
28. P. G. Taylor, A. R. Bassindale, Y. El Aziz, M. Pourny, R. Stevenson, M. B. Hursthouse and S. J. Coles, *Dalton Trans.*, 2012, **41**, 2048-2059.
29. R. Franco, A. K. Kandalam, R. Pandey and U. C. Pernisz, *J Phys Chem B*, 2002, **106**, 1709-1713.
30. M. Laird, A. Van Der Lee, D. G. Dumitrescu, C. Carcel, A. Ouali, J. R. Bartlett, M. Unno and M. Wong Chi Man, *Organometallics*, 2020, **39**, 1896-1906.
31. M. Laird, N. Herrmann, N. Ramsahye, C. Totée, C. Carcel, M. Unno, J. R. Bartlett and M. Wong Chi Man, *Angew. Chem. Int. Ed.*, 2020, **10.1002/anie.202010458**.
32. M. Laird, J. Yokoyama, C. Carcel, M. Unno, J. R. Bartlett and M. Wong Chi Man, *J Sol Gel Sci Technol*, 2020, **95**, 760-770.
33. N. Oguri, N. Takeda and M. Unno, *Chem. Lett.*, 2015, **44**, 1506-1508.
34. D. Brondani, F. H. Carré, R. J. P. Corriu, J. J. E. Moreau and M. Wong Chi Man, *Angew. Chem. Int. Ed.*, 1996, **35**, 324-326.
35. M. Unno, Y. Imai and H. Matsumoto, *Silicon Chem.*, 2003, **2**, 175-178.
36. M. Tanabe, K. Mutou, N. Mintcheva and K. Osakada, *Organometallics*, 2008, **27**, 519-523.
37. M. Syroeshkin, Y. Wang, M. Dieng, V. Gul'Tyai and V. Jouikov, *ECS Transactions*, 2013, **45**, 29-38.
38. M. Ronchi, S. Sulaiman, N. R. Boston and R. M. Laine, *Appl. Organomet. Chem.*, 2010, **24**, 551-557.